

## Flood risk assessment for informal settlements

R. De Risi · F. Jalayer · F. De Paola · I. Iervolino · M. Giugni ·  
M. E. Topa · E. Mbuya · A. Kyessi · G. Manfredi · P. Gasparini

Received: 23 January 2013 / Accepted: 29 May 2013 / Published online: 8 June 2013  
© Springer Science+Business Media Dordrecht 2013

**Abstract** The urban informal settlements are particularly vulnerable to flooding events, due to both their generally poor quality of construction and high population density. An integrated approach to the analysis of flooding risk of informal settlements should take into account, and propagate, the many sources of uncertainty affecting the problem, ranging from the characterization of rainfall curve and flooding hazard to the characterization of the vulnerability of the portfolio of buildings. This paper proposes a probabilistic and modular approach for calculating the flooding risk in terms of the mean annual frequency of exceeding a specific limit state for each building within the informal settlement and the expected number of people affected (if the area is not evacuated). The flooding risk in this approach is calculated by the convolution of flooding hazard and flooding fragility for a specified limit state for each structure within the portfolio of buildings. This is achieved by employing the flooding height as an intermediate variable bridging over the fragility and hazard calculations. The focus of this paper is on an ultimate limit state where the life of slum dwellers is endangered by flooding. The fragility is calculated by using a logic tree procedure where several possible combinations of building features/construction details, and their eventual outcome in terms of the necessity to perform structural analysis or the application of nominal threshold flood heights, are taken into account. The logic tree branch

---

R. De Risi (✉) · F. Jalayer · I. Iervolino · G. Manfredi  
Department of Structures for Engineering and Architecture, University of Naples Federico II,  
Via Claudio 21, 80125 Naples, Italy  
e-mail: raffaele.derisi@unina.it

F. Jalayer · I. Iervolino · M. Giugni · M. E. Topa · G. Manfredi · P. Gasparini  
Analysis and Monitoring of Environmental Risk (AMRA), Scarl,  
Via Nuova Agnano 11, Naples 80125, Italy

F. De Paola · M. Giugni  
Department of Civil, Architectural and Environmental Engineering, University of Naples Federico II,  
Via Claudio 21, 80125 Naples, Italy

E. Mbuya · A. Kyessi  
Institute of Human Settlements Studies (IHSS), Ardhi University, Dar es Salaam, Tanzania

probabilities are characterized based on both the orthophoto recognition and the sample in situ building survey. The application of the methodology is presented for Suna, a subward of Dar es Salaam City (Tanzania) in the Msimbazi River basin having a high concentration of informal settlements.

**Keywords** Extreme meteorological events · Flood · Climate-related hazard · Fragility · Informal settlements · Africa

## 1 Introduction

Around half of the world's population lives in urban areas. By 2050, this ratio is estimated to rise up to around 70 % (UN Habitat 2010). One of the most significant consequences of the rapid urbanization process is the phenomenon of the squatter settlements also known as the *informal settlements*, *shanty towns*, and *slums*. Although slightly different in their definitions, these denominations all refer to generally poor standards of living. A significant proportion (around one-third) of the urban growth in the developing regions is unprogrammed and in the form of informal urban human settlements (UN Habitat 2010). The lack of formal engineering criteria in the construction of informal settlements together with their generally poor construction quality renders them particularly vulnerable to extreme natural phenomena (De Risi 2013).

It can be argued that assessment and prediction of the adverse effects of climate-related events, quantification of the vulnerability of the affected areas, and finally risk assessment are important steps in an integrated climate-related adaptation and strategic decision-making. In particular, rainfall-induced flooding can pose a serious threat to high-density urban areas; this is especially the case for informal settlements built in river banks and flood plains. The informal buildings, due to their generally poor or non-existent structural detailing and the material used for their construction, are particularly vulnerable to water infiltration and seepage during extreme rainfall and/or flooding. The flood damage to buildings can be classified into two main categories: damage due to direct contact with water and structural failure. If the material used for the foundation is not water-tight or if the foundation is on or under the ground level, or if there are no barriers built in front of the door, the water can easily come into contact with the building. In this case, if the building is not sufficiently water-tight, the water can infiltrate inside the building. This is going to lead to material deterioration and erosion, non-sanitary living conditions, and risk of drowning. On the other hand, the structural failure is more likely to take place due to hydrostatic pressure, hydrodynamic pressure, debris impact, and a combination of these actions (Kelman and Spence 2004).

In the recent years, increasing attention is focused on flooding risk assessment. In fact, several publications discuss the consequences of flooding, such as loss of life (Jonkman et al. 2008), economic losses (Pistrika 2010; Pistrika and Jonkman 2010; Pistrika and Tsakiris 2007), and damage to buildings (Smith 1994; Chang et al. 2009; Kang et al. 2005; Schwarz and Maiwald 2008; Zuccaro et al. 2012). These research efforts have many aspects in common, such as a direct link between the flooding intensity and the incurred damage and that they are based on real damage observed in the aftermath of the flooding event. On the other hand, many research efforts are starting to galvanize in the direction of proposing analytical models for flood hazard and vulnerability assessment taking into account the many sources of uncertainties. Nadal et al. (2010) propose a stochastic method

for the assessment of the direct impact of flood actions on buildings. A general methodological approach to flood risk assessment is embedded in the HAZUS procedures for risk assessment (Scawthorn et al. 2006a, b). Lacasse and Nadim (2011) have proposed various case studies on the assessment of hydro-geological risk, presenting a range of methods from simple/qualitative to more complex/quantitative approaches. Apel et al. (2009) have done a comprehensive study on the various scales of complexity and precision involved in the flood risk assessment.

This work presents an integrated modular probabilistic methodology for predicting flooding risk of spatially distributed structures in a portfolio at a detailed micro-scale (e.g., a neighborhood) in a Geographical Information System (GIS) framework. Although the methodology presented is general with respect to any structural type, it is specifically oriented toward application for the case of informal settlements. It is also particularly suitable for problem-solving based on incomplete information. This aspect is particularly evident in the construction of the rainfall curve and in data acquisition and processing for the vulnerability assessment of informal settlements.

The paper is organized into two main parts, namely the methodology and the numerical application. The first part explores in a step-by-step manner the probabilistic methodology for flooding risk assessment of structures. The proposed methodology is described in a modular manner: the rainfall-return period curves, the characterization of peak discharge and total flooding volume for each return period, the two-dimensional diffusion model for a given flood hydrograph, the assessment of building fragility to flooding for a specified ultimate limit state, and finally the calculation of flooding risk for each of the structures in the designated portfolio. The second part is dedicated to the demonstration of the proposed methodology in flooding risk assessment for the informal dwellings in Suna sub-ward in Dar es Salaam (DSM), Tanzania, where heavy rains and flooding have killed more than a dozen people and left thousands homeless in December 2011.

## 2 Methodology

### 2.1 General probability-based framework

The proposed methodology can be summarized in a single equation (Eq. 1), where  $\lambda_{LS}$  denotes the risk expressed as the mean annual rate of exceedance of a given limit state (LS). The limit state refers to a threshold (e.g., critical water height  $h_{f,c}$ , critical velocity  $v_{f,c}$ ) for a structure, beyond which, it no longer fulfills a specified functionality.  $\lambda(h_f)$  denotes the mean annual rate of exceedance of a given flooding height  $h_f$  at a given point in the considered area.  $P(LS|h_f)$  denotes the flooding fragility for limit state LS expressed in term of the probability of exceeding the limit state threshold.

$$\lambda_{LS} = \int_{h_f} P(LS|h_f) \cdot |d\lambda(h_f)| \tag{1}$$

It should be noted that the flooding fragility embodies both uncertainties in mechanical material properties and the building-to-building variability in features relevant to flooding. The risk  $\lambda_{LS}$  is calculated in terms of the mean annual frequency of exceeding the limit state LS for each node of the lattice covering the zone of interest by integrating fragility  $P(LS|h_f)$  and the (absolute value of) hazard increment  $|d\lambda(h_f)|$  over all possible values of flooding height. The mean annual frequency of exceeding the limit state  $\lambda_{LS}$  is later

transformed into the annual probability of exceeding the limit state assuming a homogeneous Poisson recurrence process.

In this work, the limit state threshold is specified based on the flood height. That is, the limit state threshold can be defined as the critical water height, beyond which the structure exceeds the limit state in question. It is helpful in this context to consider the critical water height as a proxy for the structural capacity for the specified limit state.

It should be noted that Eq. (1) manages to divide the flood risk assessment procedure into two main modules, namely the hazard assessment module which leads to the calculation of the mean annual frequency  $\lambda(h_f)$  of exceeding a given flooding height  $h_f$  and the vulnerability assessment module which leads to the calculation of the flooding fragility curve in terms of the probability of exceeding specified limit state  $P(LS|h_f)$ .

Figure 1 demonstrates a flow chart of the proposed procedure. As it can be seen, historical rainfall data are transformed into rainfall probability curves. This information together with detailed topography of the area, geology maps, and land-use maps are then used in order to evaluate the basin hydrograph and to develop the flooding hazard maps (i.e., inundation scenarios for various return periods). The vulnerability of the portfolio of informal settlements is then evaluated in terms of fragility functions for a specific limit state, based on orthophotos of the area, sample in situ building survey, and laboratory tests for mechanical material properties. Finally, the flooding risk map is obtained by integrating the flooding hazard map and the fragility functions for the informal settlements.

The proposed methodology integrates climate modeling, hydrographic basin modeling, and structural fragility modeling in order to generate the risk map for the zone of interest. In the following sections, the above-mentioned steps are described in detail.

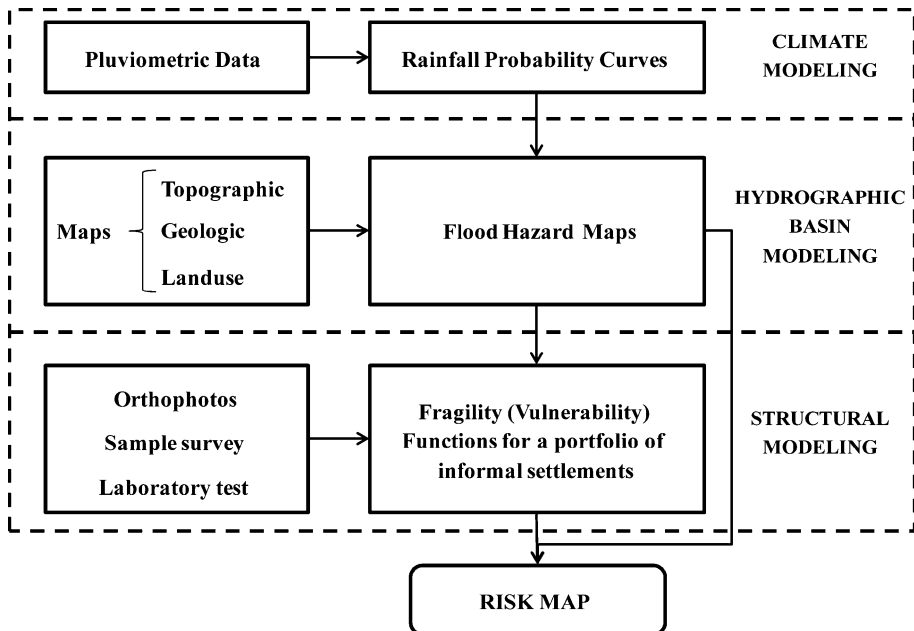


Fig. 1 Flowchart representation of the methodology

## 2.2 Climate model

Climate modeling constitutes the first step in developing a probabilistic inundation model. Its output is usually expressed in terms of rainfall scenarios for various return periods, also known as the *rainfall curves* or the *intensity–duration–frequency* (IDF) curves. The rainfall curves are normally used, in lieu of sufficient data for direct probabilistic discharge modeling, in order to evaluate the peak discharge.

This paper employs historical pluviometric data in order to obtain the rainfall curves. To evaluate the potential impact of climate change, a similar procedure can be followed employing the rainfall curves that are obtained based on the downscaling of various climate projection scenarios, if the same assumptions about the process of occurrence hold.

### 2.2.1 The rainfall curve based on incomplete historical records

IDF curve is a tool that characterizes an area's rainfall pattern. By analyzing past rainfall events, statistics about rainfall recurrence can be determined for various standard return periods ( $T_R$ ) (e.g., 2, 10, 30, 50, 100, and 300 years). The pluviometric data consist of rainfall records collected at a specific monitoring location. Rainfall intensity  $i$  is calculated as the average rainfall depth  $h_r$  that falls per time increment ( $i = h_r/d$ , with  $d$  rainfall duration) and is measured in millimeter per hour. The annual extremes are then calculated for various time windows. The rainfall curve, corresponding to a specific return period, is calculated by fitting a suitable probability model to the extreme rainfall data. Herein, a bi-parameter Gumbel probability distribution (generalized extreme value, or GEV, family of distributions) has been chosen to describe the extreme rainfall data (Maione and Moisélo 1993). It can be shown that (see Appendix 1 for detailed derivation) the rainfall intensity  $h_r$  for a given return period  $T_R$  and duration  $d$  can be calculated from a bi-parameter power-law:

$$h_r(d, T_R) = a \cdot d^n \quad (2)$$

where  $a$  and  $n$  are the parameters of the rainfall curve, which can be estimated by a simple linear regression analysis, in the bi-logarithmic scale, namely  $\log(h_r)$  versus  $\log(d)$ .

The maximum annual rainfall data for a specific duration are not always available.<sup>1</sup> In such cases, available data could be *disaggregated* to the desired durations. This involves generating synthetic sequences of rainfall for smaller time windows (e.g., 10', 30', 1 h, 3 h, 6 h, 12 h), with statistical properties equal to that of the observed daily rainfall. In this work, two alternative downscaling techniques are used in order to generate maximum rainfall values for the desired time windows. The short-time intensity disaggregation method (Connolly et al. 1998) has been used for the simulation of smaller time windows (i.e., 10', 30', 1 h), and the random cascade-based disaggregation method (Olsson 1998; Güntner et al. 2001) has been used for larger time windows (i.e., 3, 6 and 12 h).

## 2.3 Hydrographic basin model

A schematic diagram of the procedure used for hydrographic basin modeling is illustrated in Fig. 2. IDF curves, geologic and land-use information are used to characterize the

<sup>1</sup> As it was the case for the meteorological data gathered for precipitations in Dar-es-Salaam, the rainfall data available through [www.tuitempo.net](http://www.tuitempo.net) and [www.knmi.nl](http://www.knmi.nl) are reported for  $d = 24$  h for a specific year (last accessed 01/01/2013).

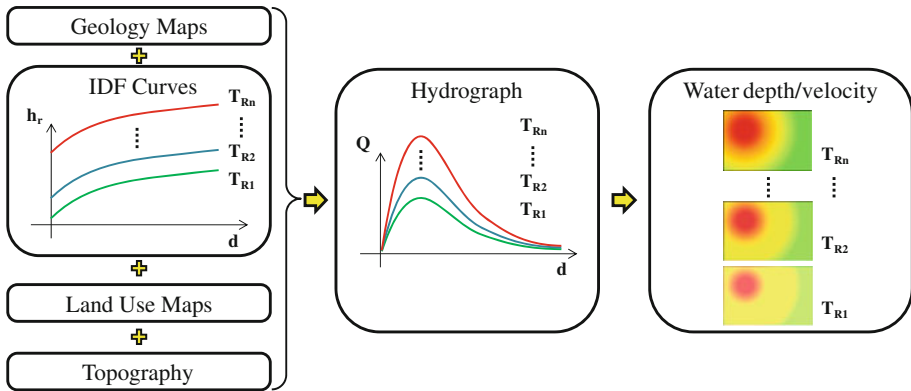


**Fig. 2** Hydrographic basin modeling procedure

hydrograph, denoted by  $Q$ , leading to the calculation of the peak discharge and the total water volume for different return periods. This information, together with the topographic map of the zone of interest, is used, in a two-dimensional diffusion model, in order to generate the maps of maximum water height and velocity, for each cell of the lattice covering the zone of interest for a given return period (the *flooding hazard map*). This procedure is described in more detail in the following.

### 2.3.1 Catchment area definition

Catchment area characterization, which is done based on the topography of the zone, is one of the very first steps in hydrographic basin analysis. The catchment refers to the topographical area from which a watercourse, or a water course section, receives surface water from rainfall (and/or melting snow or ice).

### 2.3.2 Hydrograph

Once the rainfall curve or the IDF curve has been characterized, a rainfall-runoff method must be applied in order to evaluate the hydrograph. The hydrograph refers to the flow discharge as a function of time and constitutes the input for the hydraulic diffusion model. The area under the hydrograph is equal to the total discharge volume for the basin under study. For drainage-type catchments, where water runoff cannot be directly measured, the classic curve number method (CNM) (SCS 1972) can be employed. The antecedent soil moisture condition (AMC) in the drainage catchment can influence the curve number (CN) value, and in particular, there are three classes of AMC (AMC I: the soils in the catchment are practically dry; AMC II: average condition; AMC III: the soils in the catchment are practically saturated from previous rainfalls). In this study, a CNII class corresponding to the average condition (AMCII) has been considered.

In the framework of the CNM, the characteristics of the discharge hydrograph are evaluated using a unit Mockus (SCS 1972) hydrograph depicting the discharge  $Q$  as a function of time. In particular for the evaluation of the time corresponding to the peak of the hydrograph  $t_p$  (in hours), the following formula was considered:

$$t_p = 0.5 \cdot D + t_l \quad (3)$$

where  $D$  is the rainfall duration [in hours, equal to the concentration time evaluated from Viparelli (1963)];  $t_l$  is the catchment lag time (in hours), i.e., the time between the hydrograph centroid and the net rainfall centroid, equal to:

$$t_l = 0.342 \cdot \frac{L^{0.8}}{s^{0.5}} \cdot \left( \frac{100}{CN} - 9 \right)^{0.7} \quad (4)$$

in which  $L$  is the length of main channel (in kilometers), and  $s$  is the mean slope (as percentage).

### 2.3.3 Two-dimensional propagation model

The characterization of the discharge hydrograph forms the basis for the identification of flood-prone areas. In the next step, the flood discharge estimated by the hydrograph needs to be propagated through the zone of interest in order to delineate the flood-prone areas for various return periods. In this work, flood routing in two dimensions is accomplished through the numerical integration of the equations of motion and continuity (dynamic wave momentum equation) for the flow. This has been accomplished by means of the commercial software FLO-2D (O'Brien et al. 1993; FLO-2D 2004) which is a flood volume conservation model based on general constitutive fluid equations of continuity and flood dynamics (i.e. the risk). Such two-dimensional flood simulation is based on a digital elevation model (DEM) overlaid with the surface grid, aerial photography and orthographic photos, detailed topographic maps, and digitized mapping. Such a detailed cartography is needed in order to identify the surface attributes of the grid system, for example, streets, buildings, bridges, culverts, or other flood routing or storage structures. The principal advantage in using a two-dimensional diffusion model is that it can be applied in special cases such as unconfined or tributary flow, very flat topography, and split flow.

### 2.3.4 The flood hazard curves

The two-dimensional flood routing for a given surface grid in the flood-prone area provides the values of water height and velocity for a given return period. These results can be visualized as the flood height/velocity maps for a range of return periods. Alternatively, it is possible to represent the results in terms of the flood hazard curves depicting the mean annual rate (and probability) of exceeding various flood heights/velocities for each grid point within the zone. In particular, the flood hazard curves for water height refer to the term  $\lambda(h_f)$  in Eq. (1).

### 2.3.5 Flood height as the intermediate variable

In this work, the flood height has been used as the intermediate variable (i.e., a *flood intensity measure*) linking the hydrographic basin analysis and flooding vulnerability assessment of informal settlements (see the following section). It should be noted that the one could have used also the vector consisting of the flood height and flood velocity pair. However, for the sake of tractability of calculations, it has been chosen to use the flooding

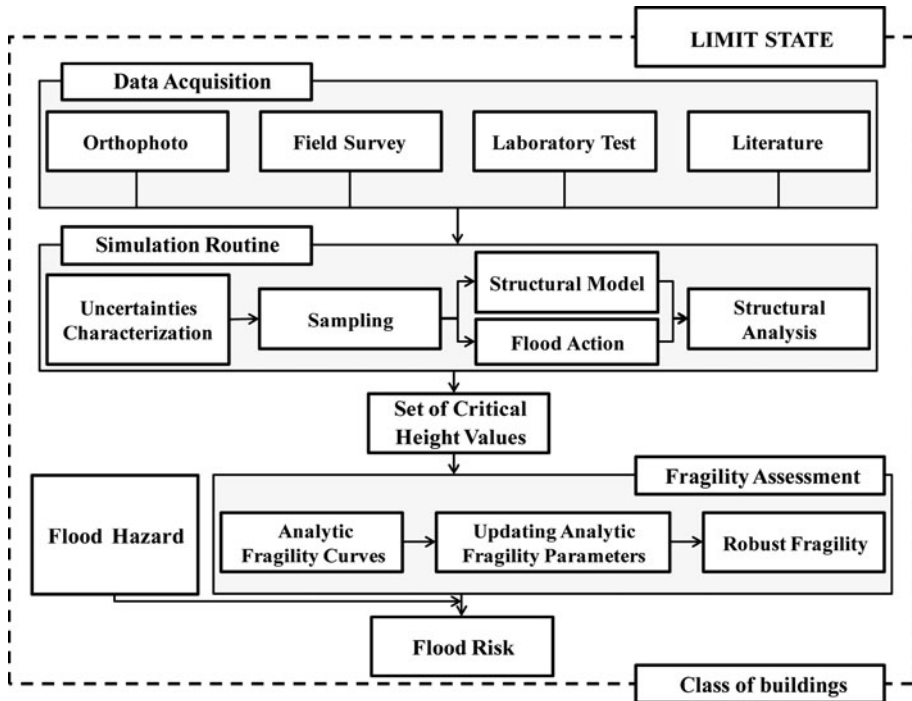


**Fig. 3** The schematic diagram of the procedure used for the assessment of the vulnerability of the class of buildings for the specific limit state

height as the only intensity measure. The flooding velocity for each point in the grid is then calculated from a power-law relation as a function of the flooding height.<sup>2</sup>

### 3 Structural fragility

The procedure employed for the assessment of the vulnerability of buildings is suitable for a portfolio of buildings which demonstrate similar features with respect to the performance of interest (i.e., they belong to the same *class* of structures, see for example, Iervolino et al. 2007). Of course, the methodology can be extended to cases where more than one class of structures can be identified. As far as it regards the application presented in this work, the informal settlements located in the same neighborhood tend to have the similar characteristics. For instance, they usually have the same number of floors, the same wall material (e.g., adobe, rammed earth or cement stabilized blocks), the same roof material (e.g., corrugated iron sheet or wooden frame), and similar geometrical patterns (De Risi et al. 2012). Therefore, the portfolio of the informal settlements located in the same neighborhood can be classified as one class of buildings. Figure 3 demonstrates a schematic diagram of the procedure used for the calculation of the fragility curves for a given class of buildings and for a prescribed structural limit state.

<sup>2</sup> This power-law relation is characterized for each point within the grid separately based on the results of flood propagation for the maximum velocity/height pairs for various return periods.



The procedure is divided into three distinct modules: (a) data acquisition, (b) simulation, and (c) fragility assessment. Each of these modules is explained in detail hereafter. The resulting fragility curve, coined also as *the robust fragility*, represents the vulnerability of the class of the buildings for the prescribed limit state. The fragility curve for the class of buildings and the prescribed limit state is then integrated together with the flooding hazard curve in order to estimate the flooding risk expressed in terms of the mean annual rate of exceeding the limit state, as per the discussed methodology. The limit state probability values can then be implemented in order to calculate the expected annual loss or the expected number of affected people.

### 3.1 The data acquisition module

The first step in the procedure employed for the assessment of the vulnerability of the class of building is the data acquisition. Ideally, it is desirable to conduct an exhaustive field survey and map out the structural details for all the buildings in the portfolio of structures considered. In the same manner, it is desirable to conduct laboratory tests that mimic the construction materials and techniques in the field, in order to evaluate the construction materials mechanical properties. However, in lieu of exhaustive field tests and relevant laboratory tests, in this work, a mix of alternative data sources has been exploited, namely orthophotos, sample field surveys, and literature results.

#### 3.1.1 The orthophoto boundary recognition

Boundary recognition based on recent orthophotos of the zone of study is used in order to determine the plan dimensions of the buildings. This consists in the graphic identification of the buildings' plan dimensions via a GIS-based procedure. This helps in obtaining the full range of building dimensions in the zone of interest. In particular, the length of the longest wall for each building is recorded in order to obtain the histogram of the wall length values throughout the portfolio.

#### 3.1.2 Sample field survey

A sample of detailed building surveys is used in order to lay out the spatial variation in building geometry and structural detailing inside the class of buildings (the sample field survey sheet is attached in Appendix 2). Data gathered from survey are processed (in the simulation module) in order to construct the joint probability distribution for structural modeling parameters. The building characteristics, deemed relevant for the vulnerability, are the wall thickness, the height of the building, the presence of barriers in front of the door or raised foundation, the quality of doors and windows (sealed or not sealed), the sizes of the doors and windows, the height of the windows from bottom and the height of the barrier or of the raised foundation (if applicable).

#### 3.1.3 Literature survey

Ideally, the structural material properties should be obtained based on the results of specific laboratory tests. The laboratory tests are aimed to mimic the construction materials and relevant techniques used in the field, in order to evaluate the elastic modulus ( $E$ ), the Poisson ratio ( $\nu$ ), and the compression ( $f_m$ ), shear ( $\tau$ ) and the out of plane flexural strength ( $f_f$ ) as well as to gain an estimate of deterioration due to elongated contact with water. Herein, in lieu of

laboratory tests, the existing literature results are used. In particular in the application presented herein, cement block material properties are taken from the existing literature.

### 3.2 The simulation module

A simulation routine is used in order to sample the building-to-building variability of structural features within the portfolio. Herein, an efficient-simulation-based procedure is employed that relies on a small number of simulations (e.g., in the order of 20-50). The final output of the simulation is a set of critical height values calculated for the simulation realizations of the uncertain parameters (described later). The simulation routine can be identified by a logic tree approach. Figure 4 illustrates a sample (simplified) logic tree defining the simulation path. For example, the logic tree illustrated in the figure states that the structural model is going to be generated only if the building is sufficiently water-proof. In this case, the type of structural model to be generated depends on the decision that the wall has a door or not. In case the building is not water-proof, the structural analysis is not going to be performed and the critical water height is going to be assigned nominally. The value of the critical water height ( $h_{f,c}$ ) is going to depend on the fact that the building has a raised platform or not, in which case it is going to be equal to a nominal (prescribed) water height ( $h_{nominal}$ ) plus the height of the platform ( $h_{platform}$ ) .

#### 3.2.1 Characterization of uncertainties

The uncertainties taken into account in the assessment of structural vulnerability can be classified into those related to material mechanical properties and those related to structural detailing and geometry. In this step, the information gathered in the data acquisition module is processed in order to develop the joint probability distribution for the set of

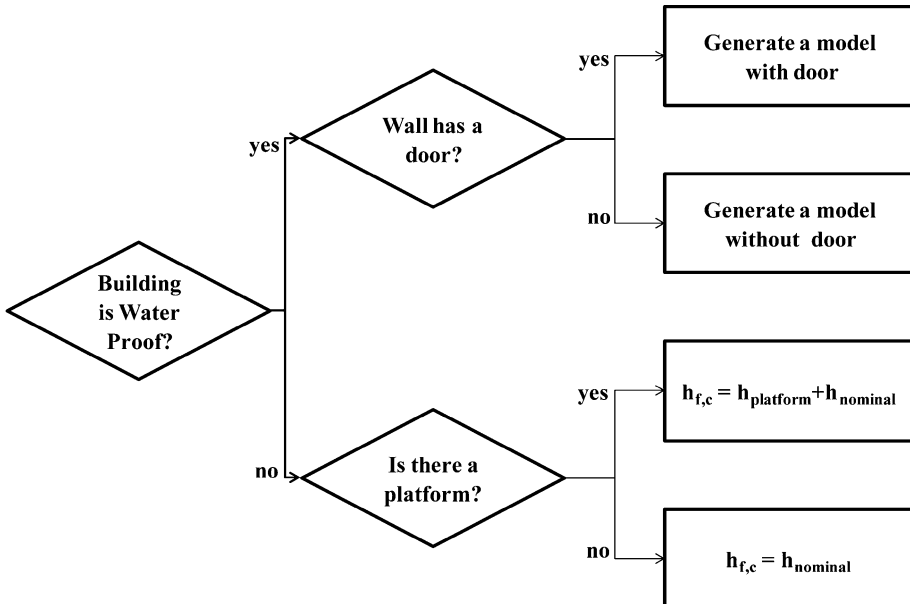


Fig. 4 The schematic diagram of a logic tree defining the simulation procedure

uncertain parameters. It is important to note that the uncertainties considered in the assessment of the fragility functions for the class of structures take into account both the lack of knowledge and the spatial variability. The generated probability distributions are going to be used to define the probabilities associated with the various branches of the logic tree. It should be noted that the logic tree approach is an effective tool for modeling possible correlations between various structural modeling parameters/features. The detailed description of the procedure for constructing the probability distribution based on the gathered data is out of the scope of this paper (see De Risi et al. 2013 for more details). However, a simple example is reported here as a demonstration. Suppose that among 50 sample surveys, 25 are revealed to have raised platforms as foundation. In this case, the probability that there is a raised platform is set to 0.50. On the other hand, the set of 25 platform heights recorded is going to be used to generate a cumulative probability function for the platform height.

### 3.2.2 Sampling

Having characterized the probability distribution for the set of uncertain parameters, a detailed logic tree can be designed in order to direct the sampling procedure. At each bifurcation of the branch where a decision has to be made, the probability values estimated in the previous step are used in order to regulate the sampling process. Back to the example laid out in the previous step, 50 % of the extractions are going to have a raised platform and the remaining extractions are not going to have a raised platform. Among the samples having a raised platform, the cumulative distribution function (CDF) constructed for the platform heights in the previous section is going to be used to generate a sample of platform heights based on this probability distribution. It is important to note that the sampling procedure is going to involve both the structural model and the flooding action (De Risi et al. 2013). In particular, the maximum flooding height considered in the structural analysis is going to change based on information whether there is water seepage through the windows. Moreover, the parameters deciding the profile of the hydro-dynamic pressure have been simulated based on the variability of velocity profile with respect to the flooding height profile in the zone of interest.

### 3.2.3 Structural analysis

For each simulation realization, a distinct structural model and loading pattern is going to be generated. Moreover, it is also going to be determined whether the structural analysis is going to be performed or nominal values are used. In case structural analyses are performed, the critical flooding height is going to be determined based on safety checking (e.g., based on admissible stress) of various control sections strategically located in the wall corners or through the openings. That is, the critical water height is going to be calculated as the minimum critical water height calculated for all the control section verified during the safety checking procedure.

## 3.3 The fragility assessment module

The simulation procedure leads to set of critical height values corresponding to each simulation realization. At this stage, one could already construct a fragility curve based on the (empirical) distribution of the critical height values. However, given the many sources

of uncertainty present in the vulnerability assessment problem, it is desirable to use these critical height values as data and construct an analytic probability model based on this data. This probability model would also lead to establishing confidence bands (as a function of the number of simulations) on the resulting fragility curve which is going to be the expected value of the various plausible analytic fragility curves and we have coined it herein as the *robust fragility* (Jalayer et al. 2011; Papadimitriou et al. 2001). In the following, the various steps leading to the estimation of robust fragility and its confidence band are described.

### 3.3.1 The analytic fragility curve

Based on what was said before about the different outcomes on the structure being water-proof or not in terms of performing structural analysis or assigning nominal values, the following analytical model is adopted:

$$F(h_f|\pi, \eta, \beta) = P(h_{f,c} \leq h_f) = \pi \cdot \Phi\left(\frac{\ln \frac{h_f}{\eta}}{\beta}\right) + (1 - \pi) \cdot I(h_f) \tag{5}$$

where the parameters  $\pi$ ,  $\eta$ , and  $\beta$  reported after the conditioning sign (|) are the three parameters that define the analytic probability distribution/fragility function.  $\pi$  is the probability that the structure is sufficiently water-tight;  $\eta$  is the median critical water height given that the structure is sufficiently water-tight; and  $\beta$  is the logarithmic standard deviation for the critical water height, denoted by  $h_{f,c}$ , given that the structure is sufficiently water-tight.  $\Phi(\cdot)$  denotes the standard Gaussian (Normal) cumulative probability distribution and  $I(h_f)$  is an indicator function defined as follows:

$$I(h_f) = \begin{cases} 0 & \text{if } h_f \leq h_{\text{nominal}}(\text{LS}) \\ 1 & \text{if } h_f > h_{\text{nominal}}(\text{LS}) \end{cases} \tag{6}$$

depicting a step function identified by the nominal water height ( $h_{\text{nominal}}(\text{LS})$ ) corresponding to the limit state under consideration. Figure 5a illustrates  $I(h_f)$ . Note that  $I(h_f)$  can also be interpreted as the Dirac delta function at  $h = h_f$ .

The analytical fragility model proposed in Eq. (5) can be interpreted as an application of the total probability theorem (Benjamin and Cornell 1970) on the two mutually exclusive outcomes marked by probability  $\pi$  that the structure is water-tight or not. In case the structure is water-tight, the structural analyses are going to be performed and a lognormal probability distribution with parameters  $\eta$  and  $\beta$  seems adequate for describing the variability in the critical water height values, as shown in Fig. 5b. Otherwise, a nominal critical

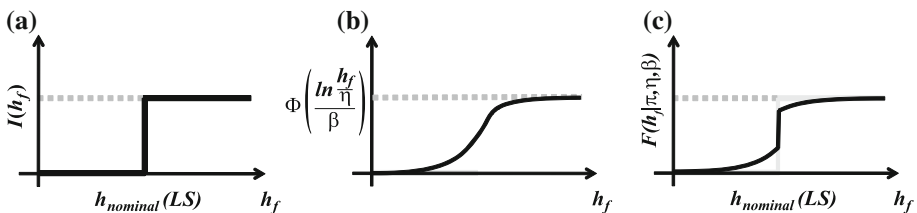


**Fig. 5** **a** Fragility expressed as a step function when the structure is not water-tight; **b** Fragility function given that the structure is water-tight; **c** The resulting analytical fragility curve (see Eq. 5)

water height is going to be assigned and the step function illustrated in Fig. 5a is adopted. Figure 5c illustrates the empirical critical heights values together with the analytical fragility model proposed in Eq. (5).

### 3.3.2 Updating analytical fragility parameters

Denoting the parameters of the analytic fragility function as  $\chi = [\pi, \eta, \beta]$ , the joint probability distribution for the vector of parameters  $\chi$  can be referred to as  $p(\chi)$ . Using Bayesian updating, the probability distribution for the parameters of the fragility function can be updated using formulas described in (Box and Tiao 1992) based on the set of critical height values obtained from simulation. The updated probability distribution can be denoted as  $p(\chi|H_c)$  where  $H_c$  is the vector of critical height values obtained through simulation. This probability distribution has a twofold utility: in the first place, it identifies the maximum likelihood estimates of the fragility function parameters given data  $H_c$ , and in the second place, it considers the uncertainty in the vector  $\chi$  due to limited number of simulations.

### 3.3.3 The robust fragility

Finally, the robust fragility is calculated as the expected value of the analytic function  $F(h_f|\chi)$  in Eq. (5) over the entire domain of vector  $\chi$  and according to the updated joint probability distribution  $p(\chi|H_c)$ :

$$F(h_f|H_c) = E[F(h_f|\chi)] = \int_{\Omega} F(h_f|\chi) \cdot p(\chi|H_c) \cdot d\chi \tag{7}$$

where  $E[.]$  is the expected value operator and  $\Omega$  is the domain of the vector  $\chi = [\pi, \eta, \beta]$ . The variance  $\sigma^2$  in fragility estimation can be calculated as:

$$\sigma^2 [F(h_f|\chi)] = E[F(h_f|\chi)^2] - E[F(h_f|\chi)]^2 \tag{8}$$

where  $E[F(h_f|\chi)^2]$  can be calculated from Eq. (7) replacing  $F(h_f|\chi)$  with  $F(h_f|\chi)^2$ .

## 4 Risk assessment

Point estimates of the flooding risk can be obtained by integrating the robust fragility for the class of structures and the flood hazard in Eq. (1). In this case, the flooding risk is expressed in terms of the mean rate of exceeding the structural limit state (i.e., exceeding the critical flooding height corresponding to the limit state in question) for a given point. The annual probability of exceeding a limit state  $P(\text{LS})$ , assuming a homogeneous Poisson process model with rate  $\lambda_{\text{LS}}$ , can be calculated as:

$$P(\text{LS}) = 1 - \exp(-\lambda_{\text{LS}}) \tag{9}$$

The exposure to risk can be quantified by calculating the total expected loss or the expected number of people affected for the portfolio of buildings.

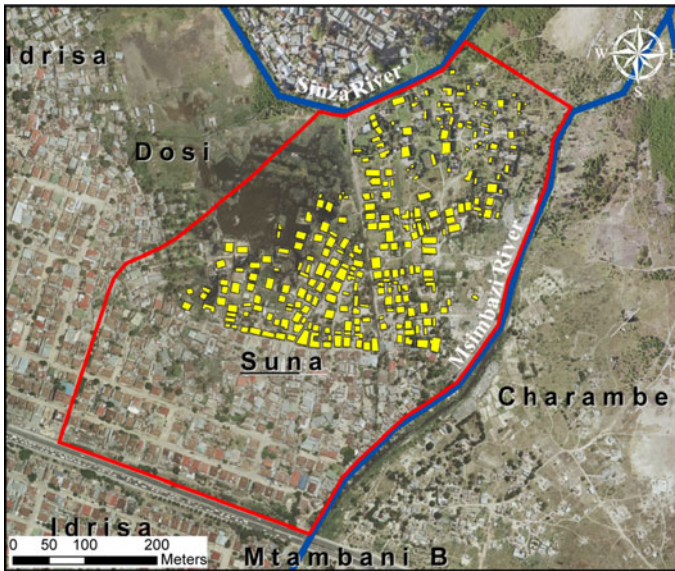


**Fig. 6** The case study area and the portfolio of the buildings studied

#### 4.1 Expected loss

The expected repair costs<sup>3</sup> (per building or per unit residential area),  $E[R]$ , can be calculated as a function of the limit state probabilities and by defining the damage state  $i$  as the structural state between limit states  $i$  and  $i + 1$ :

$$E[R] = \sum_{i=1}^{N_{LS}} [P(LS_{i+1}) - P(LS_i)] \cdot R_i \quad (10)$$

where  $N_{LS}$  is the number limit states that are used in the problem in order to discretize the structural damage;  $R_i$  is the repair cost corresponding to damage state  $i$ ; and  $P(LS_{N_{LS}+1}) = 0$ .

#### 4.2 Expected number of people affected

The expected number of people affected by flooding can also be estimated as a function of the limit state probabilities from Eq. (10) replacing  $R_i$  by the population density (per house or per unit residential area).

### 5 Case study

The case study focuses on flood risk assessment for the informal settlements located in the *Suna sub-ward*, shown in Fig. 6, in the Kinondoni District in DSM, Tanzania. Suna, located on the western bank of the Msimbazi River with an extension of about 50 ha, is a

<sup>3</sup> It should be mentioned that, in principle, the expected loss should/could also take into account the contribution of the costs related to, for example, end of life, relocation, and maintenance.

historically flood-prone area. The Msimbazi River flows across Dar es Salaam City from the higher areas of Kisarawe in the Coastal region and discharges into the Indian Ocean.

### 5.1 The rainfall curve

The rainfall curve is obtained based on historical rainfall data (from 1958 to 2010) from a single meteorological station located in the DSM International Airport at 55 m.a.s.l. and 6°86′ latitude and 39°20′ longitude. Based on these recordings, the mean annual rainfall for DSM city can be estimated at around 1,110 mm. The IDF curve is obtained by following the procedure outlined in Sect. 2.2.1 and is characterized by the following relationship:

$$h_r(d, T_R) = K_{T_R} \cdot 36.44 \cdot d^{0.25} \tag{11}$$

The values of the growing factor  $K_{T_R}$  are:  $K_2 = 0.95, K_{10} = 1.42, K_{30} = 1.70, K_{50} = 1.83, K_{100} = 2.01, K_{300} = 2.29$ .

The rainfall curves classified by six different return periods are plotted in Fig. 7.

### 5.2 The definition of the catchment area

The first step in the delineation of inundated areas in the Suna district was the definition of the catchments of the Msimbazi River and its main tributaries. Three different catchments (of about 250 km<sup>2</sup>) were identified as shown in Fig. 8.

The characteristics of the three catchments identified are reported in Table 1. The land-use and geological maps are illustrated in Fig. 9a, b, respectively. From the geological point of view, the catchments are characterized mainly by clay-band sands and gravels (corresponding to soil group B in the Curve Number method). With reference to the land use, catchment 1 and 2 are characterized mainly by agricultural use and catchment 3 is characterized as residential area.

### 5.3 The characterization of the hydrographs

The peak flow of the three catchments was evaluated by the Curve Number method, with reference to six different return periods (e.g., 2, 10, 30, 50, 100, and 300 yr). The inflow

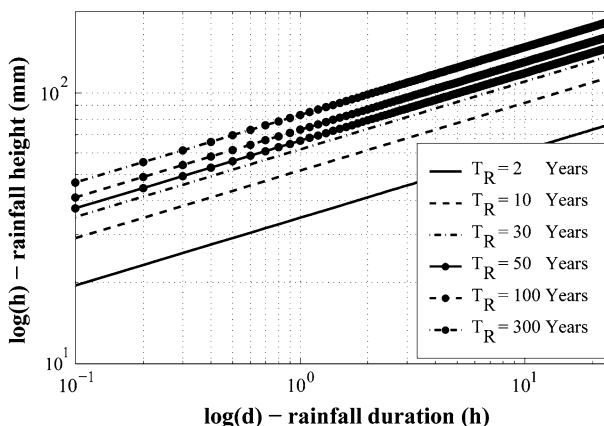
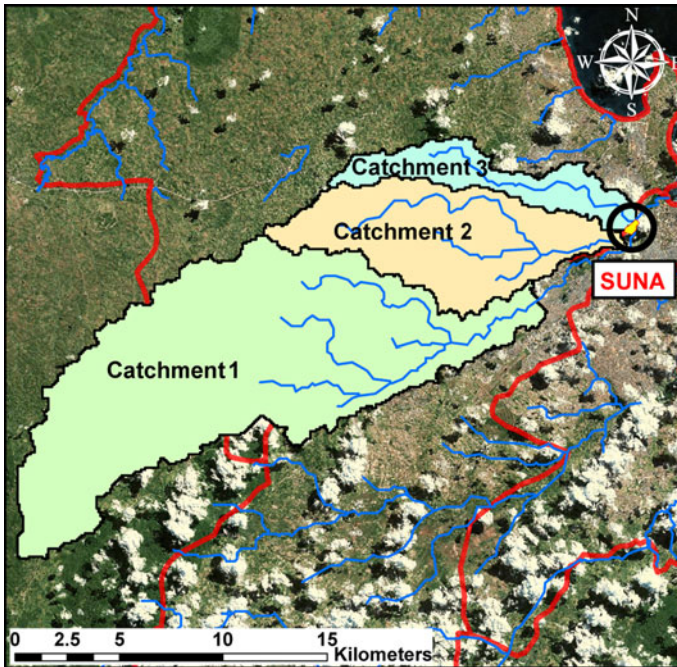


Fig. 7 Rainfall probability curves for Dar es Salaam





**Fig. 8** Visualization of the Mzimbazi catchments with the position of the case study area

**Table 1** The characteristics of the Mazimbazi River catchments

Characteristics	Msimbazi River		
	Catchment 1	Catchment 2	Catchment 3
Drainage area (km <sup>2</sup> )	166.3	60.5	24.1
Main channel length (km)	32.7	18.2	14.9
Average slope (%)	5.8	4.2	3.9
Average height (m.a.s.l.)	175.5	108.6	97.2
CNII	64.73	77.98	89.91
$t_p$ (h)	13.03	6.90	4.63

hydrographs for catchment 1 corresponding to the various return periods considered are illustrated in Fig. 10.

#### 5.4 The flood hazard

The software FLO-2D was used for a bi-dimensional simulation of the propagation of the flooding volume based on the calculated hydrographs and a digital elevation model (DEM) assuming a 45 h simulation time. The outcome of the flood propagation is illustrated in Fig. 11, in terms of maximum flow depth  $h_{\max}$  (in meters), with reference to the six considered return periods. The flood hazard curves, plotting the mean annual rate of exceeding various flooding heights (i.e., inverse of the return period), are illustrated in Fig. 12a. Each curve



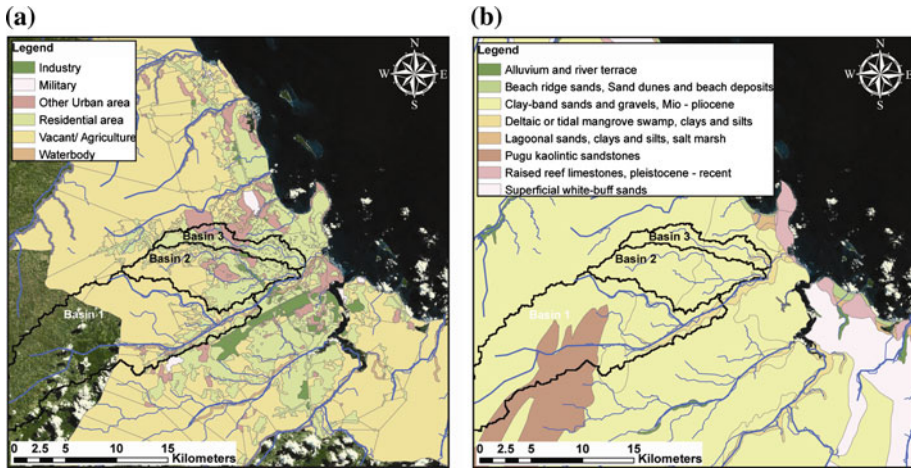
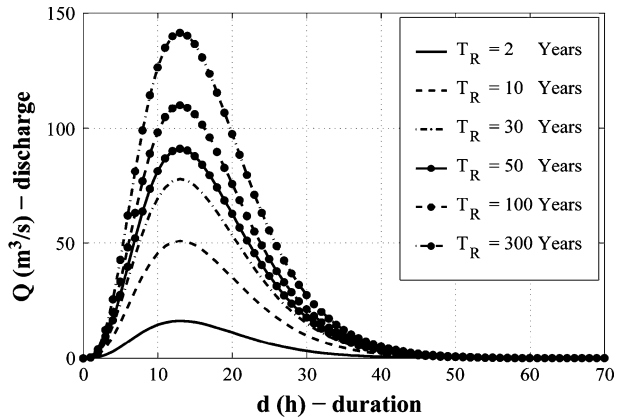


**Fig. 9** Mzimbazi River catchments: **a** Land use, **b** Geology

**Fig. 10** Hydrographs evaluated for catchment 1 ( $T_R = 2, 10, 30, 50, 100$  and  $300$  years)



maps to the centroid of a building belonging to the portfolio of the buildings considered. For each building centroid and each return period considered, the  $h_{max} - v_{max}$  pairs and the power-law relation fitted to them are plotted in Fig. 12b. It should be mentioned that the quantified results reported in this section are corroborated by evidence gathered in two field trips made to the zone of study. This evidence includes presence of several water ponds from relatively recent rainfall events, visual signs of degradation due to contact with water in the buildings (e.g., capillary rise), and qualitative testimony of the inhabitants regarding periodicity and intensity of flooding events in the area.

### 5.5 The structural limit state

Risk assessment is performed for the limit state of life safety. This limit state marks an ultimate state of the structure in which the lives of the inhabitants are going to be in danger. This can be caused either due to the presence of water inside the building or due to the collapse of the walls.

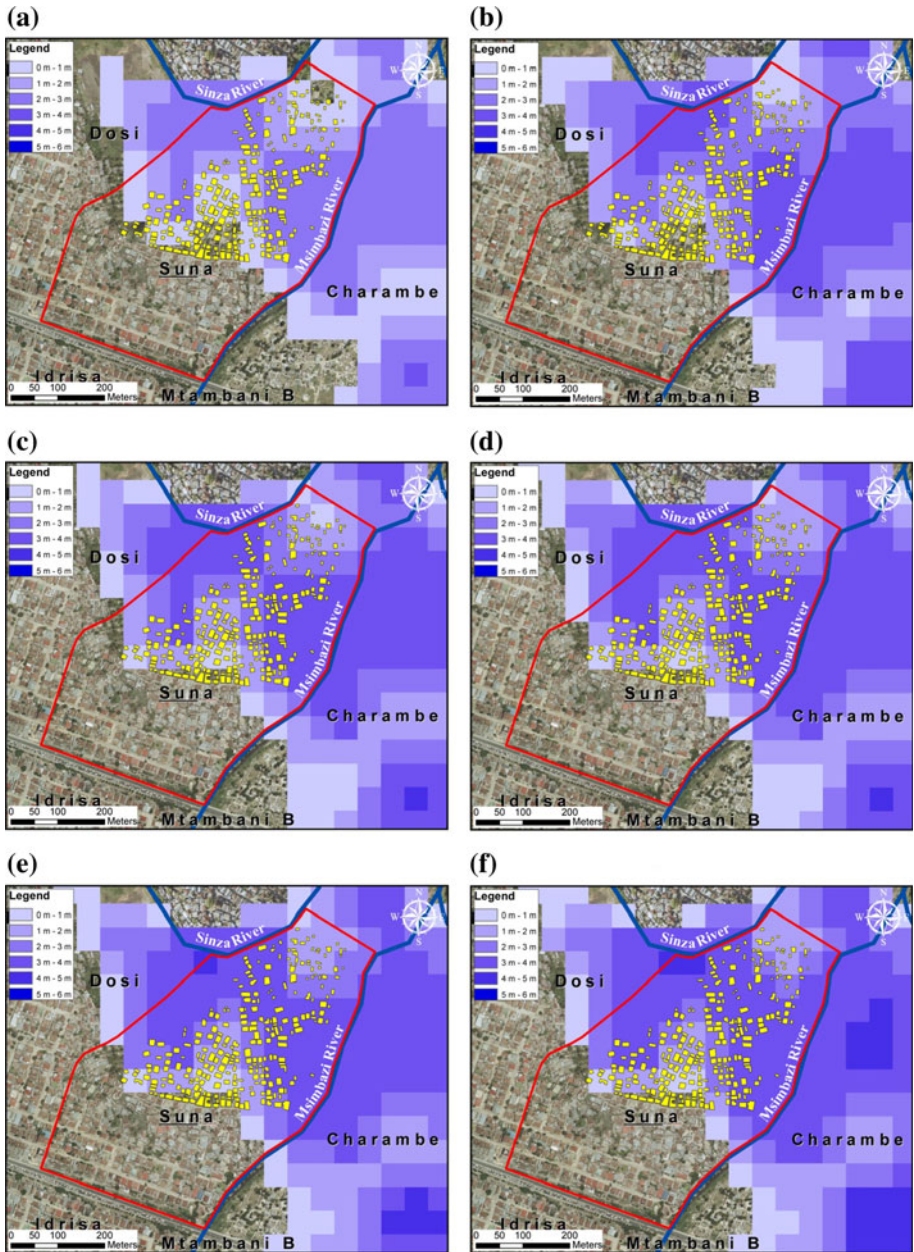


**Fig. 11** Inundation profiles for different return periods in terms of  $h_{\max}$ : **a**  $T_R = 2$  years, **b**  $T_R = 10$  years, **c**  $T_R = 30$  years, **d**  $T_R = 50$  years, **e**  $T_R = 100$  years, **f**  $T_R = 300$  years

## 5.6 Data acquisition

The portfolio of buildings is identified by overlaying the map of the case study areas with flood profiles depicted in Fig. 5b. The GIS-based boundary recognition procedure provides

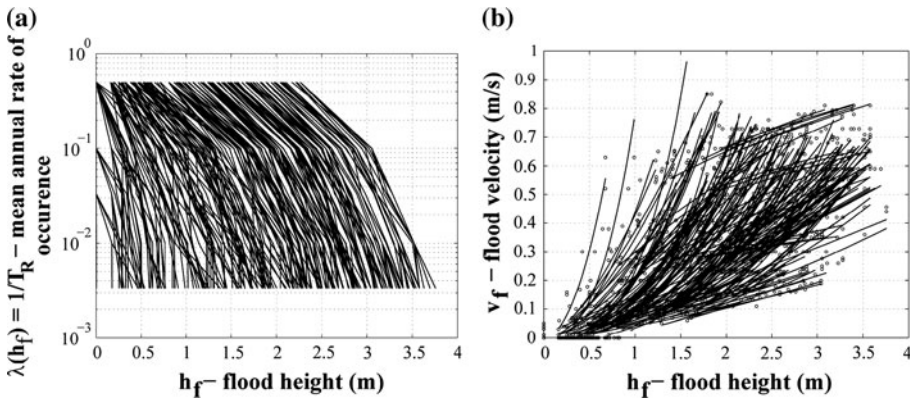


**Fig. 12** **a** Flood hazard curves in terms of maximum flood-height; **b** Correlation between maximum flood height and flood velocity

the plan dimensions for each building in the portfolio of buildings considered. The sample survey is based on 50 compiled survey sheets. Based on these results, it can be observed that buildings have more-or-less similar characteristics in terms of construction material used for walls and roof. Almost all of the buildings seem to be constructed with 460 × 230 × 125 mm cement blocks; wooden or iron beams are used as roof beams covered by corrugated iron sheets. Moreover, the blocks are systematically placed in such a way that the wall thickness observed throughout the surveyed buildings is around 140 mm (including the width of the plaster). Two types of doors have been used in the area, wooden doors and iron doors. While the former seem to be quite ineffective in preventing infiltrations, the latter seems to be more-or-less effective in preventing the flow of water from entering. In general, given the warm climate, the windows are without glass and are covered by wired net or sheets of plastic which seem quite ineffective in preventing infiltrations. As adaptation strategies, the use of cement barriers or cement raised foundation/platforms can be identified. The material mechanical properties are based on existing literature for cement hollow bricks with a voids percentage between 45 and 65 % and are reported in Table 2.

5.7 The characterization of uncertainties

Tables 3, 4, and 5 report the uncertain parameters considered in the evaluation of the fragility for the class of buildings considered classified as parameters related to qualitative information on structural detailing, quantitative geometric details, and mechanical material properties, respectively.

The qualitative structural detailing parameters depicted in Table 3 are characterized by a percentage rate (reported in table) that is estimated as the frequency of observing the

**Table 2** Cement stabilized bricks available in literature (De Risi et al. 2012)

Material type	$f_m$ (MPa) Min–Max		$\tau_0$ (MPa) Min–Max		$E$ (MPa) Min–Max		$G$ (MPa) Min–Max		$\gamma$ (kN/m <sup>3</sup> )
Hollow space 45–65 %	1.5	2.0	0.095	0.12	1,200	1,600	300	400	12
Hollow space <45 %	3.0	4.4	0.18	0.24	2,400	3,520	600	880	14

**Table 3** Qualitative structural detailing parameters

Walls with doors	25 %
Walls with windows	75 %
Rate of openings per linear meter	33 %
Structures with water-tight door	30 %
Structures with water-tight window	30 %
House with barrier in front to the door	50 %
House with raised foundation	50 %
Rate of degradation due to elongated contact water	75 %

**Table 4** Quantitative structural detailing parameters

Geometrical property	Distribution type	Mean/min	Standard deviation/max
$L$ (m)—wall length	Normal	11.17	3.39
$H$ (m)—wall height	Uniform	2.50	3.50
$t$ (m)—wall thickness	Deterministic	0.125	0.00
$L_w$ (m)—window length	Uniform	0.80	1.20
$H_w$ (m)—window height	Uniform	0.80	1.00
$H_{wfb}$ (m)—window rise	Uniform	0.80	1.20
$L_d$ (m)—door length	Uniform	0.80	1.20
$C_d$ (m)—corner length	Uniform	0.80	0.90
$H_b$ (m)—barrier height	Uniform	0.10	1.00
$H_f$ (m)—foundation rise	Normal	0.45	0.15

**Table 5** Parameters related to material mechanical properties

Mechanical properties	Distribution type	Mean/min	Standard deviation/max
$f_m$ (MPa)—compression strength	Uniform	1.50	2.00
$\tau$ (MPa)—shear strength	Uniform	0.095	0.12
$E$ (MPa)—linear elastic modulus	Uniform	1,200	1,600
$G$ (MPa)—shear elastic modulus	Uniform	500	667
$\gamma$ (kN/m <sup>3</sup> )—self-weight	Uniform	11	13
$R_f$ —flexural strength factor	Uniform	5	10

quality in question in the survey results. These rates are later going to be used as probability values identifying various branches of the logic tree used for simulations assuming stochastic independence<sup>4</sup> between structural detailing parameters. Table 4 reports the quantifiable structural detailing parameters and the probability distributions assumed. As

<sup>4</sup> As mentioned in Sect. 3.1, in the general case, uncertain parameters are not stochastically independent and the joint probability distribution would be required to characterize them. The independence assumption taken in this application herein does not harm generality of the proposed methodology, yet allows to use marginal distributions in the simulation.

mentioned before, information about the length of the structural wall  $L$  for each building is calculated by orthophoto boundary recognition as the maximum plan dimension detected. The normal probability distribution for wall length in Table 4 is characterized based on the histogram of the wall length values for all the buildings in the portfolio.

Uniform distribution is used when data are available only on the range of a variable (i.e., a lower and an upper bound). It can be noted that the thickness is taken as a deterministic value equal to the thickness of the cement bricks (125 mm). The parameters of the normal probability distributions for the height of the raised platform or the barrier are obtained based on the histogram of the observed data from the survey results.

The parameters related to the mechanical properties of the materials are reported in Table 5. The uniform distribution min/max values are obtained based on the existing literature. No correlation among the parameters has been considered. The flexural strength reduction factor denoted by  $R_f$  denotes the factor ratio of flexural strength to compression strength and normally varies between 1/5 and 1/10. If a given simulation realization is classified as degraded due to elongated contact with water (75 % of the cases, as shown in Table 3), the mechanical properties as shown in Table 5 are reduced to the 75 % of their value.<sup>5</sup>

## 5.8 Structural models and simulation

The structural model developed herein consists of a single panel of elastic shell finite elements modeled using the OpenSees software (McKenna et al. 2004). It is assumed that the panel is clumped (fixed) at the base and hinged at the two sides. The clumped restraint in the base is representative of a good wall-foundation connection; meanwhile, the hinge restraint on the two sides represents a fair transversal connection between two orthogonal walls. Based on the uncertain parameters related to the geometrical properties of the buildings, four different types of structural models are generated. These models are distinguished based on the type, number and relative positioning of openings (door and windows). Figure 13 illustrates the various configurations generated in the simulation procedure. The parameters indicated in figure are described in Table 4. In order to simulate the effect of the roof on the upper part of the wall, a vertical load equal to 0.5 kN/m and a horizontal load equal to 0.05 kN/m have been applied.

A set of critical height values are calculated from standard Monte Carlo simulation with a limited number of samples ( $n = 50$ ). The simulation is based on a logic tree, where the probability of each branch is determined based on the rate values reported in Table 3; it is to establish whether the structural model in the current realization is water-tight or not (see Appendix 3 for the complete logic tree). If the structure is water-tight, the critical water height is determined through structural analysis. Otherwise, pre-defined nominal values are assigned. The nominal value adopted in this study for the life-safety limit state is equal to 1 m.

### 5.8.1 Determination of the critical water height by structural analysis

In order to calculate the critical flood height that the wall panel can resist, the flooding height is increased in a step-by-step manner. The structural assessments for each (increasing) flooding height considered consist of checking whether the section forces exceed the corresponding section resistance for the critical sections considered (i.e., base

<sup>5</sup> This is a nominal value assigned in lieu of laboratory test results.



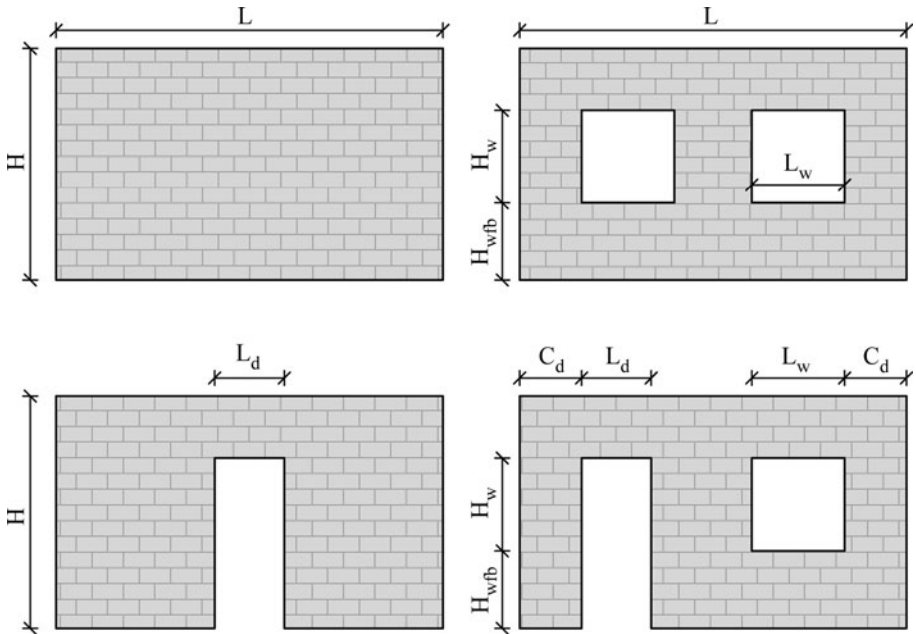


**Fig. 13** Various structural configurations considered in the analysis (see Table 4)

sections, hinged vertical sections, horizontal sections under and on the openings, vertical sections near the openings, and the mid-vertical section). The maximum water height considered for the calculation of the hydrostatic pressure is also determined from the logic tree as the water height beyond which the structure ceases to be water-tight.

### 5.9 The flood vulnerability/risk assessment

The robust fragility curve and its plus/minus one standard deviation confidence interval are calculated based on the set of critical height values determined through simulation from Eqs. (7) and (8) and plotted in Fig. 14. The figure superimposes the fragility curves with the hazard curves corresponding to the centroid of each building considered. Finally the flooding risk can be calculated integrating the fragility and the hazard as stated in Eq. (1). The light gray lines, which correspond to a return period less than 2 years, indicate that the hazard data have been calculated by linear extrapolation. The risk evaluated in terms of mean annual rate of exceeding the life-safety limit state for the case study area is reported in Fig. 15.

It can be observed that many structures have an annual frequency of exceeding the critical flood height larger than one. This indicates that on average, assuming that the structure is going to be reconstructed each time that it is collapsed, the structure is going to collapse more than once a year due to flooding. This is consistent with the high flooding values expected as showed in Fig. 11, for example, the flooding height corresponding to a return period of 2 years is around 2.5 m. The annual probability of exceeding the life-safety limit state is calculated from Eq. (9) and plotted in Fig. 16. The differences observed in terms of annual rate and probability of exceeding a prescribed limit state (Figs. 15, 16) are directly attributable to the variability in the flood hazard for the buildings studied; this

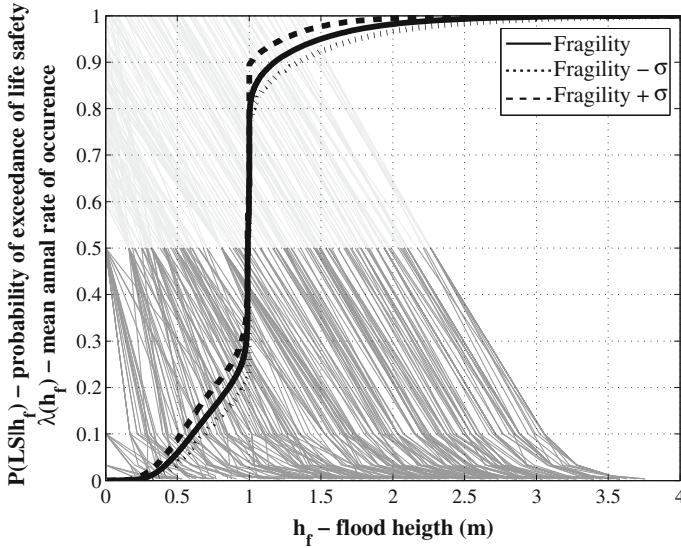


Fig. 14 Superposition of fragility curves and hazard curves

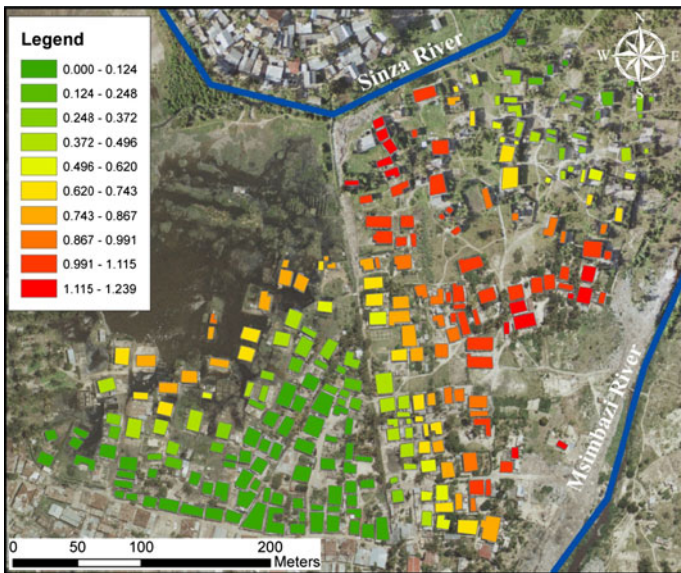
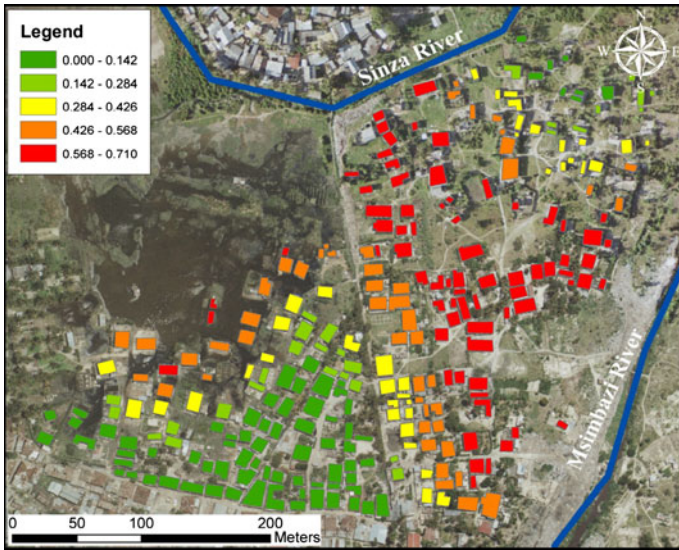


Fig. 15 The mean annual rate of exceeding the life-safety limit state

is because a common fragility curve for the entire portfolio is employed. The building-to-building variability in flood hazard which can be detected from the inundation profiles in Fig. 11 is highly sensitive to the local topography and elevation contours. Finally, the annual expected repair cost is calculated from Eq. (10) summed up over all the buildings within the portfolio of structures considering only the life-safety limit state. In this case, the repair cost per unit area corresponding to the life-safety limit state is assumed to be equal



**Fig. 16** Annual probability of exceeding the life-safety limit state for Suna sub-ward

to the replacement/reconstruction costs of  $5\$/m^2$ . The total area of the buildings within the portfolio is already calculated through the orthophoto boundary recognition. The total annual expected cost normalized by the total cost of reconstruction of the entire portfolio is equal to 35 %.

Assuming a population density of 0.03 per unit area, the expected number of people affected by flooding in one year is calculated to be 227 over 658, this is equal to 35 % of the total estimated number of people living in the case study area. In Figs. 17 and 18 are shown the results in terms of people affected and economical losses, respectively, considering the uncertainties in the fragility assessment. Neglecting other sources of uncertainties (e.g., the modeling uncertainties related to hazard estimation, the uncertainties in estimating the exposure), the expected losses are estimated be variable between 33 % (corresponding to fragility  $- \sigma$ ) and 36 % (corresponding to fragility  $+ \sigma$ ) of the total exposure in the interested area. It is worth mentioning that the building-to-building variability observed in and the expected number of people affected in a year and the expected annual repair costs (Figs. 17, 18) are due to variations in both flood hazard and exposure

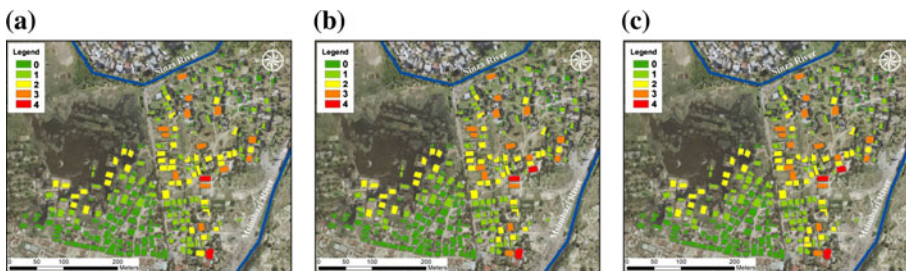


**Fig. 17** Expected number of people annually affected by flooding corresponding to **a** fragility  $- \sigma$ , **b** fragility, and **c** fragility  $+ \sigma$



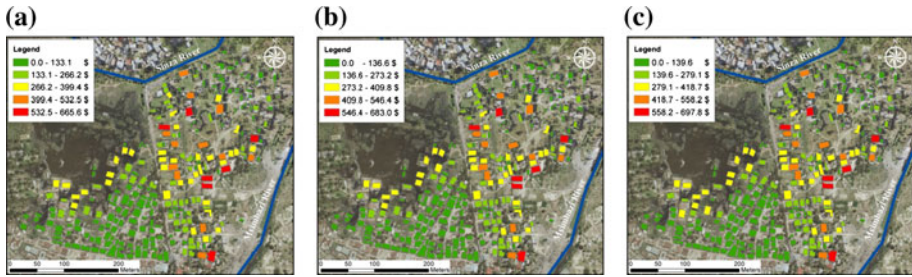


**Fig. 18** Expected annual repair costs per each buildings relatives to **a** Fragility –  $\sigma$  **b** Fragility and **c** Fragility +  $\sigma$

(this latter is taken as proportional to the plan area of each building extracted from orthophotos).

### 6 Conclusion

An integrated modular approach to flood risk assessment for structures in a portfolio of informal settlements is proposed. It integrates climate modeling, hydrographic basin modeling, and structural fragility modeling in order to generate the risk maps for the zone of interest.

Historical extreme rainfall data are transformed, via the characteristics of the catchments and the topographical information, into flood heights and velocity for various nodes within the zone of interest for different return periods. This also leads to site-specific flooding hazard curves as a function of flood heights.

A simulation-based procedure is presented for the assessment of the vulnerability of a portfolio of informal settlements to flooding. This procedure is particularly efficient when the portfolio of buildings can be characterized as a single class of buildings. This is normally the case with informal dwellings. The vulnerability of the portfolio of structures is represented by the fragility curve and the confidence interval built around it in order to take into account the limited number of simulations used in the procedure. Vulnerability assessment is focused on the limit state of life safety which is defined as an ultimate state in the structure when the life of its inhabitants is in danger and is identified by critical water height values. In case, the structure under examination is revealed not to be sufficiently water-tight (common in informal settlements), a pre-defined nominal value is assigned to the critical water height.

The flooding risk is expressed as the annual probability of exceeding the structural limit state of interest, and it is obtained by integrating the flood and fragility curves over the entire range of possible flooding heights. The total expected repair costs and the expected number of people affected by flooding can also be calculated based on the annual limit state probabilities.

An application to the *Suna sub-ward* of Dar es Salaam illustrates the methodology. The case study assessment is focused on the limit state of life safety which is defined as an ultimate state in the structure when the life of its inhabitants is in danger. It is worth mentioning that this methodology is quite suitable for being codified as an automatic procedure. In fact, the authors have also developed a software platform based on this methodology (see De Risi et al.

2013). Thus, this methodology can also be applied in order to make flood risk assessment for the informal settlements in other urban contexts in Africa.

It is to finally note that the presented quantitative approach, novel with respect to flood risk management, was developed specifically for informal settlements, yet it is general with respect to building typology and can be extended to make assessments for a portfolio of buildings consisting of multiple classes of structures.

**Acknowledgments** This work was supported in part by the European Commission's seventh framework program Climate Change and Urban Vulnerability in Africa (CLUVA), FP7-ENV-2010, Grant No. 265137. This support is gratefully acknowledged.

### Appendix 1: Estimating the parameters of the intensity–duration–frequency (IDF) curves

The IDF curves can be characterized by two or three parameters, as shown in the following expressions:

$$h_r(d, T_R) = a(T_R) \cdot d^n \quad (12)$$

$$h_r(d, T_R) = \frac{a(T_R) \cdot d}{(b + d)^c} \quad (13)$$

in which  $T_R$  is the return period and  $a(T_R)$ ,  $b$ ,  $c$ , and  $n$  are the parameters that have to be estimated through a probabilistic approach. In the present study, the power-law curves expressed in (12) have been used. Herein, a Gumbel probability distribution (belonging to the GEV family of distributions) has employed, considering only the extreme events on a block fixed window (Maione and Moisello 1993) to fit the extreme rainfall data:

$$P(h_r) = \exp\{-\exp[-u(h_r - v)]\} \quad (14)$$

where  $P(h_r)$  is cumulative distribution function (CDF) for  $h_r$ . The parameters of the Gumbel distribution are related to the sample mean  $\mu$  and sample standard deviation  $\sigma$  through the following equations:

$$u = 1.28/\sigma \quad (15)$$

$$v = \mu - 0.45 \cdot \sigma \quad (16)$$

The inverse of CDF (14) can be calculated by calculating  $h$  in terms of  $P(h_r)$  and duration  $d$ :

$$h_r(d, P) = v - \ln[-\ln(P)]/u \quad (17)$$

Substituting (15) and (16) and introducing the variation coefficient  $CV$  equal to  $\mu/\sigma$ :

$$h_r(d, P) = \mu(d) \cdot \left\{ 1 - CV(d) \cdot \left[ 0.45 + \frac{1}{1.28} \cdot \ln[-\ln(P)] \right] \right\} \quad (18)$$

Since the probability  $P$  is related to the return period  $T_R$ ,  $h$  can be expressed in terms of the return period:

$$h_r(d, T_R) = \mu(d) \cdot [1 + CV(d) \cdot K] \tag{19}$$

where<sup>6</sup>

$$K = -\left\{ 0.45 + \frac{1}{1.28} \cdot \ln \left[ -\ln \left( 1 - \frac{1}{T_R} \right) \right] \right\} \tag{20}$$

The experimental evidence also shows that extreme precipitations have a physical property, known as scale invariance, such that holds the following relation:

$$h_r(T_R, sf \cdot d) / h_r(T_R, d) = (sf)^n \tag{21}$$

in which *sf* is a scale factor and *n* is a parameter function of the location. It can be shown that this scale invariance implies the statistical self-similarity between the probability distribution of  $h_r(d)$  and  $h_r(sf \cdot d)$ . Applying the scale invariance by means of the bound method, an equal value of *n* can be imposed for any return period  $T_R$  (Chow et al. 1988). As a result of the statistical self-similarity,  $\mu(d) = a_\mu \cdot d^n$ , in which  $\mu(d)$  is the mean value for the Gumbel distribution. Substituting the expression for  $\mu(d)$  in Eq. (19), one obtains the flood height as function of duration *d* and return period  $T_R$ :

$$h_r(d, T_R) = a_\mu \cdot d^n \cdot (1 + CV_m \cdot K) \tag{22}$$

Taking into account the general expression (12), the above equation can be written as:

$$h_r(d, T_R) = a(T_R) \cdot d^n$$

where  $a(T_R)$  can be calculated as:

$$a(T_R) = a_\mu \cdot K_{T_R} \tag{23}$$

where  $K_{T_R} = (1 + CV_m \cdot K)$ .  $K_{T_R}$  is generally known as the *growing factor* (with  $T_R$ ).  $CV_m$  denotes the mean CV over different durations *d*. For a variation coefficient slightly variable with the duration *d*, the mean value  $CV_m$  can be evaluated by the following expression:

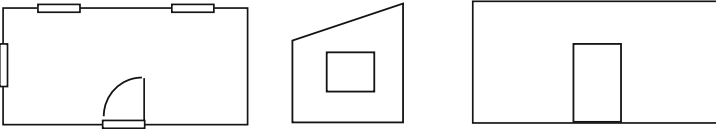

$$CV_m = \frac{1}{k} \cdot \sum_{i=1}^k CV_i \tag{24}$$

in which *k* is the considered duration, generally equal to 5, (e.g., refers to  $d = 1, 3, 6, 12,$  and 24 h) in our study *k* is equal to 7 (refers to  $d = 10', 30', 1 \text{ h}, 3 \text{ h}, 6 \text{ h}, 12 \text{ h}, 24 \text{ h}$ ).

### Appendix 2: The sample field survey sheet

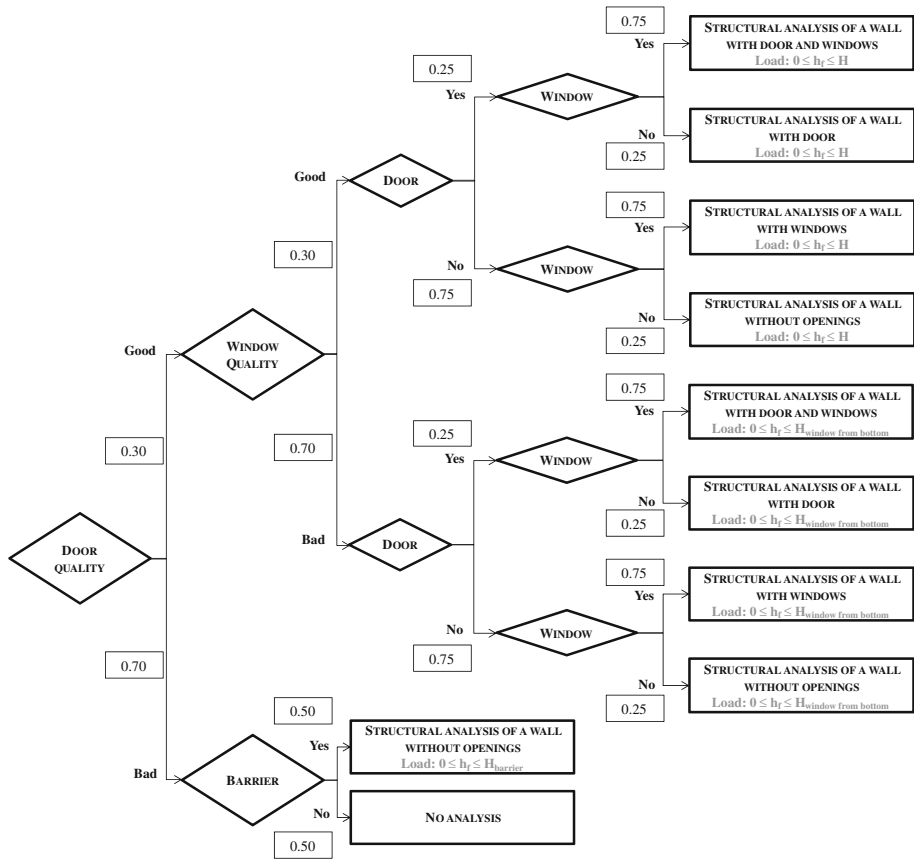
A typical survey sheet filled during the phase of data acquisition in the field, Suna subward, Dar Es Salaam (See Sect. 5.5).

<sup>6</sup> Note that the return period  $T_R$ , defined here as a function of non-exceedance probability *P*, can be numerically close to the return period for a homogenous Poisson process with rate  $(I - P)$  for sufficiently large return periods.

PLAN VIEW WITH EXTERNAL SIZE					
					
PHOTO 1		PHOTO 2			
					
GPS Coordinates		06° 48.316' S    39° 15.974' E			
N° of stories	1	Height of story	3.55 m		
Presence of Mezzanine (Mansard)		Yes	<input type="checkbox"/>		
		No	<input checked="" type="checkbox"/>		
Geometrical size					
L (plan Length)	8.00 m	W (plan width)	3.40 m		
Wall Material	Cement Blocks				
Wall Thickness	0.125 m				
Presence of cross connection in the corners	Yes	<input checked="" type="checkbox"/>	No		
			<input type="checkbox"/>		
Presence of buttresses	Yes	<input type="checkbox"/>	No		
			<input checked="" type="checkbox"/>		
Presence of plaster	Yes	<input type="checkbox"/>	No		
			<input checked="" type="checkbox"/>		
Presence of water-proof paint	Yes	<input type="checkbox"/>	No		
			<input checked="" type="checkbox"/>		
If the wall material is wood and mud:	Are the wooden piles anchored in foundation?		Yes		
			<input type="checkbox"/>		
	Are the wooden horizontal piles connected and continuous over the perimeter?		Yes		
			<input type="checkbox"/>		
Roof Typology	Flat	<input type="checkbox"/>	Pitch	<input checked="" type="checkbox"/>	
				One Side	<input checked="" type="checkbox"/>
				Two Side	<input type="checkbox"/>
	Structural Material (a)	Corrugated Iron			
	Presence of roof beams	Yes	<input checked="" type="checkbox"/>	If yes, material (b):	
				wood	
	Presence of drainage or drip	Yes	<input type="checkbox"/>	No	<input checked="" type="checkbox"/>
Presence of roof coverage	Yes	<input type="checkbox"/>	If yes, material (c):		
Use of waterproof Material	Yes	<input type="checkbox"/>	If yes, material:		
	No	<input type="checkbox"/>	Yes	<input checked="" type="checkbox"/>	
Presence of foundation	If yes:				
	Construction material		stone		
	Elevation from ground		0.00 m		
Presence of lintel beam	Yes		<input checked="" type="checkbox"/>		
			<input type="checkbox"/>		
Functionality of doors and windows (in impeding/delaying the water entrance)	Quality of the doors:	Good	<input type="checkbox"/>	Bad	<input checked="" type="checkbox"/>
					<input checked="" type="checkbox"/>
Quality of the windows:	Good	<input type="checkbox"/>	Bad	<input checked="" type="checkbox"/>	
				<input checked="" type="checkbox"/>	
Minimum height of the windows above the floor	1.20 m				
Window dimensions	L (plan Length)	1.23 m	H (height)	1.20 m	
Height of the door above the floor	0.00 m				
Door dimensions	L (plan Length)	1.22 m	H (height)	1.95 m	
Presence of barrier in front of the door	No	<input type="checkbox"/>	Yes	<input checked="" type="checkbox"/>	
	If yes:				
	Elevation from ground		1.00 m		

### Appendix 3: Logic tree

The detailed logic tree used in a simulation-based procedure for constructing the fragility curve (see Sect. 3.2).



**References**

Apel H, Aronica GT, Kreibich H, Thieken AH (2009) Flood risk analyses—how detailed do we need to be? *Nat Hazard* 49:79–98

Benjamin JR, Cornell CA (1970) *Probability, statistics, and decision for civil engineers*. McGraw-Hill, New York

Box GEP, Tiao GC (1992) *Bayesian inference in statistical analysis*. Wiley Interscience, New York

Chang LF, Kang JL, Su MD (2009), Depth-damage curve for flood damage assessments industrial and commercial sectors. In: *Proceedings of the 4th IASME/WSEAS international conference on water resources, hydraulics & hydrology*

Chow VT, Maidment DR, Mays LW (1988) *Applied hydrology*. McGraw-Hill, New York

Connolly RD, Schirmer J, Dunn PK (1998) A daily rainfall disaggregation model. *Agric For Meteorol* 92:105–117

De Risi R (2013) *A probabilistic bi-scale frame work for urban flood risk assessment*. PhD dissertation. Department of structures for Engineering and Architecture, University of Naples Federico II, Naples

De Risi R, Jalayer F, Iervolino I, Kyessi A, Mbuya E, Yeshitela K, Yonas N (2012) Guidelines for vulnerability assessment and reinforcement measures of adobe houses, CLUVA project deliverable D2.4. Available at [http://www.cluva.eu/deliverables/CLUVA\\_D2.4.pdf](http://www.cluva.eu/deliverables/CLUVA_D2.4.pdf). Accessed 24 Dec 2012

De Risi R, Jalayer F, Iervolino I, Manfredi G, Carozza S (2013) VISK: a GIS-compatible platform for micro-scale assessment of flooding risk in urban areas. In: *Papadarakakis M, Papadopoulos V, Plevis V (eds) COMPDYN, 4th ECCOMAS Thematic conference on computational methods in structural dynamics and earthquake engineering*. Kos Island, Greece

FLO-2D Software, Inc. 2004. FLO-2D® User’s Manual, Nutrioso, Arizona, [www.flo-2.com](http://www.flo-2.com)

- Güntner A, Olsson J, Calver A, Gannon B (2001) Cascade-based disaggregation of continuous rainfall time series: the influence of climate. *Hydrol Earth Syst Sci* 5:145–164
- Iervolino I, Manfredi G, Polese M, Verderame GM, Fabbrocino G (2007) Seismic risk of R.C. building classes. *Eng Struct* 29(5):813–820
- Jalayer F, Elefante L, Iervolino I, Manfredi G (2011) Knowledge-based performance assessment of existing RC buildings. *J Earthq Eng*. doi:10.1080/13632469.2010.501193
- Jonkman SN, Vrijling JK, Vrouwenvelder ACWM (2008) Methods for the estimation of loss of life due to floods: a literature review and a proposal for a new method. *Nat Hazard* 46:353–389
- Kang JL, Su MD, Chang LF (2005) Loss functions and framework for regional flood damage estimation in residential area. *J Mar Sci Technol* 13(3):193–199
- Kelman I, Spence R (2004) An overview of flood actions on buildings. *Eng Geol* 73(3–4):297–309
- Lacasse S, Nadim F (2011) Learning to live with geohazards: from research to practice. *Geotechnical Special Publication* 224:64–116
- Maione U, Moisello U (1993) Elementi di statistica per l'idrologia. La Goliardica Pavese
- McKenna F, Mazzoni S, Scott MH, Fenves GL (2004) Open system for earthquake engineering simulation (OpenSEES) (version 1.7.4). Pacific Earthquake Engineering Research Center, University of California at Berkeley. <http://opensees.berkeley.edu>
- Nadal NC, Zapata RE, Pagán I, López R, Agudelo J (2010) Building damage due to riverine and coastal floods. *J Water Resour Plan Manag* 136(3):327–336
- O'Brien JS, Julien PY, Fullerton WT (1993) Two-dimensional water flood and mudflow simulation. *J Hydraul Eng* 119(2):244–261
- Olsson J (1998) Evaluation of a cascade model for temporal rainfall disaggregation. *Hydrol Earth Syst Sci* 2:19–30
- Papadimitriou C, Beck JL, Katfygiotis LS (2001) Updating robust reliability using structural test data. *Probab Eng Mech* 16(2):103–113
- Pistrika AK (2010) Flood damage estimation based on flood simulation scenarios and a GIS platform. *Eur Water* 30:3–11
- Pistrika AK, Jonkman SN (2010) Damage to residential buildings due to flooding of New Orleans after hurricane Katrina. *Nat Hazard* 54:413–434
- Pistrika A, Tsakiris G (2007), Flood risk assessment: a methodological framework, water resources management: new approaches and technologies, European Water Resources Association, Chania, Crete, Greece, 14–16 June
- Scawthorn C, Blais N, Seligson H, Tate E, Mifflin E, Thomas W, Murphy J, Jones C (2006a) HAZUS-MH flood loss estimation methodology. I: overview and flood hazard characterization. *Nat Hazards Rev.* 7, SPECIAL ISSUE: Multihazards Loss Estimation and HAZUS, 60–71
- Scawthorn C, Flores P, Blais N, Seligson H, Tate E, Chang S, Mifflin E, Thomas W, Murphy J, Jones C, and Lawrence M (2006b) HAZUS-MH flood loss estimation methodology. II. Damage and loss assessment. *Nat Hazards Rev.* 7, SPECIAL ISSUE: Multihazards Loss Estimation and HAZUS, 72–81
- Schwarz J, Maiwald H (2008) Damage and loss prediction model based on the vulnerability of building types. In: 4th International symposium of flood defence, Toronto, Canada, May 6–8
- Smith DI (1994) Flood damage estimation—a review of urban stage-damage curves and loss function. *Water SA* 20(3):231–238
- Soil Conservation Service (1972) National engineering handbook, Section 4, Hydrology. Department of Agriculture, Washington, 762 p
- UN-HABITAT, State of the World's Cities 2010/2011, Bridging The Urban Divide. Report ID 2917. <http://www.unhabitat.org/pmss/listItemDetails.aspx?publicationID=2917>. 2010
- Viparelli C (1963) Ricostruzione dell'idrogramma di piena. *L'Energia Elettrica* 6:421–428 (in Italian)
- Zuccaro G, Santo A, Cacace F, De Gregorio D, Di Crescenzo G (2012) Building vulnerability assessment under landslides actions: Castellammare di Stabia case study. *Rend. Online Soc. Geol. It., Vol 21* (2012), pp 470–472. Società Geologica Italiana, Roma 2012. ISSN 2035-8008